Biomarkers

ISSN: 1354-750X (Print) 1366-5804 (Online) Journal homepage: https://www.tandfonline.com/loi/ibmk20

Comparative study of nano and bulk Fe_3O_4 induced oxidative stress in Wistar rats

Utkarsh A. Reddy, P. V. Prabhakar & Mohd Mahboob

To cite this article: Utkarsh A. Reddy, P. V. Prabhakar & Mohd Mahboob (2018) Comparative study of nano and bulk Fe_3O_4 induced oxidative stress in Wistar rats, Biomarkers, 23:5, 425-434, DOI: 10.1080/1354750X.2018.1443508

To link to this article: https://doi.org/10.1080/1354750X.2018.1443508

Accepted author version posted online: 19 Feb 2018.
Published online: 01 Mar 2018.

BIOMARKERS
2018, VOL. 23, NO. 5, 425–434
https://doi.org/10.1080/1354750X.2018.1443508

Taylor & Francis
Taylor & Francis Group

RESEARCH ARTICLE

Comparative study of nano and bulk Fe_3O_4 induced oxidative stress in Wistar rats

Utkarsh A. Reddy#, P. V. Prabhakar and Mohd Mahboob#

Toxicology Unit, Pharmacology and Toxicology Division, Indian Institute of Chemical Technology, Hyderabad, Telangana, India

ABSTRACT

Context: Magnetic nanomaterials (Fe_3O_4 NMs) have become novel tools with multiple biological and medical applications because of their biocompatibility. However, adverse health effects of these NMs are of great interest to learn.

Objective: This study was designed to assess the size and dose-dependent effects of Fe_3O_4 NMs and its bulk on oxidative stress biomarkers after post–subacute treatment in female Wistar rats.

Methods: Rats were daily administered with 30, 300 and 1000 mg/kg b.w. doses for 28 d of Fe_3O_4 NMs and its bulk for biodistribution and histopathological studies.

Results: Fe_3O_4 NMs treatment caused significant increase in lipid peroxidation levels of treated rats. It was also observed that the NM treatment elicited significant changes in enzyme activities of superoxide dismutase, catalase, glutathione peroxidase, glutathione reductase and glutathione-S-transferase in treated rat organs with major reduction in glutathione content. Metal content analysis revealed that tissue deposition of NM in the organs was higher when compared to bulk and caused histological changes in liver.

Conclusion: This study demonstrated that for same dose, NM showed higher bioaccumulation, oxidative stress and tissue damage than its bulk. The difference in toxic effect of Fe_3O_4 nano and bulk could be related to their altered physicochemical properties.

ARTICLE HISTORY
Received 29 August 2017
Revised 15 February 2018
Accepted 17 February 2018

KEYWORDS
Fe_3O_4 nanomaterials; rat; oxidative stress; antioxidant enzymes; biodistribution; histopathology

Introduction

Nanotechnology, one of the leading and most promising technology of the twenty-first century, involves design, production and use of materials sized between 1 and 100 nm (Foth *et al.* 2012). Their controllable tiny size gives nanomaterials (NMs) unique chemical, mechanical, optical and biological properties, which provide greater potential for industrial, agricultural and medical applications (Zhu *et al.* 2008). With the rapid development and advantages of nanotechnology, NMs are rapidly replacing their larger counterparts, currently over 1600 consumer products in the market (www.nanotechproject.org). A new generation of Fe_3O_4 NMs has multifunctional applications in the field of diagnostic and therapeutic functions (Li *et al.* 2017). The transverse relaxation property of Fe_3O_4 NMs is extensively utilized in magnetic resonance imaging (MRI) and drug delivery systems (Cha *et al.* 2017). For example, Feridex, Resovist and Endorem are Fe_3O_4 NMs-based MRI contrast agents approved for clinical use by US Food and Drug Administration (Novotna *et al.* 2012). Moreover, surface functionalization of Fe_3O_4 NMs for magnetic hyperthermia gives additional properties for combinatorial therapy of cancer with a new type of biocompatible, cationic peptide dendrimers (Nigam *et al.* 2017). Zhao *et al.* (2014) used Fe_3O_4 NMs-labeled bone marrow mesenchymal stem cells (BMSCs) to trace liver healing after hepatoectomy. They are also used in early detection of cancer and thrombosis, photothermal tumor ablation, liposomes, targeted drug delivery and biosensing applications (Bekaroğlu *et al.* 2017, Gogoi *et al.* 2017, Kurbanoglu *et al.* 2017, Liu *et al.* 2017, Shen *et al.* 2017). Fe_3O_4 NMs are extensively used in nanoremediation process in treating contaminated water and soil (Hjorth *et al.* 2017). Moreover, the electrostatic adsorption properties of Fe_3O_4 NMs were well explored to purify heavy metal contaminants like Chromium (VI) and Arsenic (III and V) (Lu *et al.* 2017, Siddiqui and Chaudhry 2017).

The extensive production and consumer exposure to a variety of nanotechnology inventions has stimulated attention regarding the health concerns of human exposure to NMs, environmental contamination and ecosystem disturbance has become another apprehension. NMs possess an increased surface to volume ratio, which brings much higher reactivity and uptake compared to their bulk materials and hence they behave differently in biological system, even at the same dose (Haase *et al.* 2012).

Recent studies reported that Fe_3O_4 NMs treatment caused developmental toxicity in larval stages of *Artemia salina* (Zhu *et al.* 2017). Fe_3O_4 NMs used in denitrification process can affect the microorganism's community by attacking its cell

CONTACT Mohd Mahboob mahboobm1983@gmail.com Toxicology Unit, Pharmacology and Toxicology Division, Indian Institute of Chemical Technology, Hyderabad, Telangana 500 007, India
#Utkarsh A. Reddy and Mohd Mahboob are responsible for statistical design/analysis. utkarshreddy@gmail.com (U. A. Reddy); mahboobm1983@gmail.com (M. Mahboob).

membrane through generating reactive oxygen species (ROS) (Ma *et al.* 2017). Moreover, Fe_3O_4 NMs can cause mitochondrial damage, Golgi and endoplasmic reticulum stress resulting in induction of autophagy in the kidney and spleen of mice (Zhang *et al.* 2016). Naqvi *et al.* (2010) and Ramesh *et al.* (2012) have demonstrated that Fe_3O_4 NMs significantly enhanced ROS generation which lead to cell injury and death in macrophage and lung epithelial cells, respectively. Furthermore, mice exposed to Fe_3O_4 NMs via intra-peritoneal route for 1 week significantly induced oxidative stress in liver and kidney (Ma *et al.* 2012). Moreover, Reddy *et al.* (2017) reported oxidative stress condition in major organs of rats after sub-acute treatment of Iron oxide nanoparticles (IONPs) (Fe_2O_3 NPs). Similarly, Srinivas *et al.* (2012) showed that rat lung tissue markedly suffered oxidative stress, inflammation and histomorphological alterations following acute inhalation exposure of Fe_3O_4 NMs.

We hypothesized that the difference in the physicochemical properties of Fe_3O_4 NMs and bulk will have difference in inducing oxidative stress. Hence, we aimed to assess the size and dose-dependent biodistribution and resultant changes in oxidative stress biomarkers and histomorphology in rats after repeated oral treatment of Fe_3O_4 NM and bulk. However, the data regarding exposure levels of Fe_3O_4 NMs to humans in day-to-day life are unavailable. Hence for the present study, OECD guideline 407 was followed to draw the dose levels for assessing toxicity of both Fe_3O_4 NMs and bulk. The doses considered according to this guideline may not necessarily represent the concentrations of Fe_3O_4 NMs and bulk present in the environment, however, may provide useful information regarding possible health hazards after getting exposed to these materials.

Clinical significance

- Considering the ever increasing commercial application of Fe_3O_4 NMs in nanomedicine, these NMs should be used cautiously while studies are conducted to assess the risks they pose to human health.
- Assessment of oxidative stress biomarkers by Fe_3O_4 NMs and its bulk in female Wistar rats after repeated oral exposure emphasises size and dose-dependent effects of NMs and bulk on organs will help to advance the designing and manipulation of these NMs for further biomedical use.

Materials and methods

Materials

Fe_3O_4 NMs (cat no. 637106, 97% purity), bulk Fe_3O_4 (cat. No. 310069, 95% purity) Iron standard (cat no. 43149) and all other chemicals used in this study were procured from Sigma Aldrich Co. (St. Louis, MO).

Characterization of nanoparticles

The Fe_3O_4 NMs size and morphology was characterized using on a Hitachi H-7600 tungsten-tip transmission electron microscope (TEM). Alcohol suspension of NMs was deposited on TEM grids covered with formvar. The mean size and standard deviation were calculated by measuring over 100 NMs in random fields of view. The hydrodynamic diameter and zeta potential of Fe_3O_4 NMs in water were measured by dynamic light scattering (DLS) and laser Doppler velocimetry (LDV) using Malvern Zetasizer Nano-ZS instrument. Fe_3O_4 NMs were suspended in MilliQ water and sonicated for 10 min using sonicator (Hielscher Ultrasonics, Teltow, Germany). The polydispersity index (PDI) given is a measure of the size ranges present in the solution. Fe_3O_4 NMs and bulk were analyzed for purity using inductively coupled plasma optical emission spectrometry using standard protocol (ICP-OES, IRIS Intrepid II XDL, Thermo Jarrel Ash).

Animals and treatment

The 8–10-week-old female albino Wistar rats were bought from the National Institute of Nutrition, Hyderabad, India. Literature survey of conventional toxicological studies shows that usually there is little difference in sensitivity between the sexes, but in those cases where differences are observed, females are generally slightly more sensitive. Hence, female rats were used in our study. Standard environment of 22 °C (±2 °C) temperature, 50–60% relative humidity and 12 h light/dark cycle was maintained in animal house. AIN-93 composition has been given as pellet diet and water were supplied *ad libitum*. The test animals were kept individually in polypropylene cages with steel cover lid and were acclimatized to laboratory conditions for 7 d. All the animal experiments were endorsed by (Ref. No. IICT/BIO/TOX/PG/31/05/2016) the Institutional Animal Ethics Committee of Indian Institute of Chemical Technology, Hyderabad, India.

The study design was based on OECD (Organization for Economic Cooperation and Development) guideline 407 (2008). Fe_3O_4 NMs and bulk were suspended in water and sonicated for 15 min using probe sonicator. Control group was treated with tap water. Experimental groups (5 rats/group) were treated orally with Fe_3O_4 NMs and Fe_3O_4 bulk each at 30, 300 and 1000 mg/kg body weight (b.w) doses. The rats were treated once a day in a single dose to the animals, for 28 d using stomach tube. The volume did not exceed 1 ml/100 g body weight. The high dose was selected with the intention of bringing toxic effects but no death, medium dose was to establish dose response and lowest dose level to show no observed adverse effects (NOAEL). Rats were observed daily for toxic symptoms and behavioral changes. After 28 d, rats were sacrificed using carbon dioxide asphyxiation. Liver, kidney and brain were collected, perfused with cold potassium chloride buffer (1.15% KCl and 0.5 mM EDTA) and homogenized in potassium phosphate buffer (KPB 0.1 M, pH 7.4). The homogenate was centrifuged at 15,000 rpm for 30 min. The clear supernatant was collected and stored in aliquots in −85 °C. Protein estimation was done using Lowry *et al.* (1951) method with slight modifications.

Oxidative stress markers

Lipid peroxidation (LPO) was assessed in tissue homogenate following the method of Wills (1969). In total, 2 ml of 0.375%

thiobarbituric acid (TBA) – 15% trichloro acetic acid (TCA) reagent and 0.5 ml of tissue homogenate were taken in a tube and boiled in water bath for 30 min. The tubes were cooled, 3 ml of butanol was added to extract pink-colored TBARS (thiobarbituric acid reactive substances) complex. The absorbance was measured at 532 nm using Spectramax spectrophotometer (Molecular Devices, San Jose, CA).

The reduced glutathione (GSH) content was measured following the method of Jollow *et al.* (1974). Tissue homogenate and 4% sulfosalicylic acid were mixed in 1:1 ratio, kept in ice for 1 h and centrifuged at 10,000 rpm for 10 min. A total of 1 ml supernatant, 0.4 ml 5,5-dithiobis-2-nitrobenzoic acid (DTNB) (4 mg/ ml) and 1.6 ml KPB were taken in a tube. The yellow color developed was read at 412 nm.

Superoxide dismutase activity was estimated in tissue supernatant using the method of Marklund and Marklund (1974). A total of 45 µl of 10 mM pyrogallol and 100 µl tissue supernatant were taken in a tube and the volume was made up to 3 ml with 50 mM Tris–HCl buffer (pH 8.2) containing 1 mM DTPA (diethylene-triaminepenta acetic acid). The rate

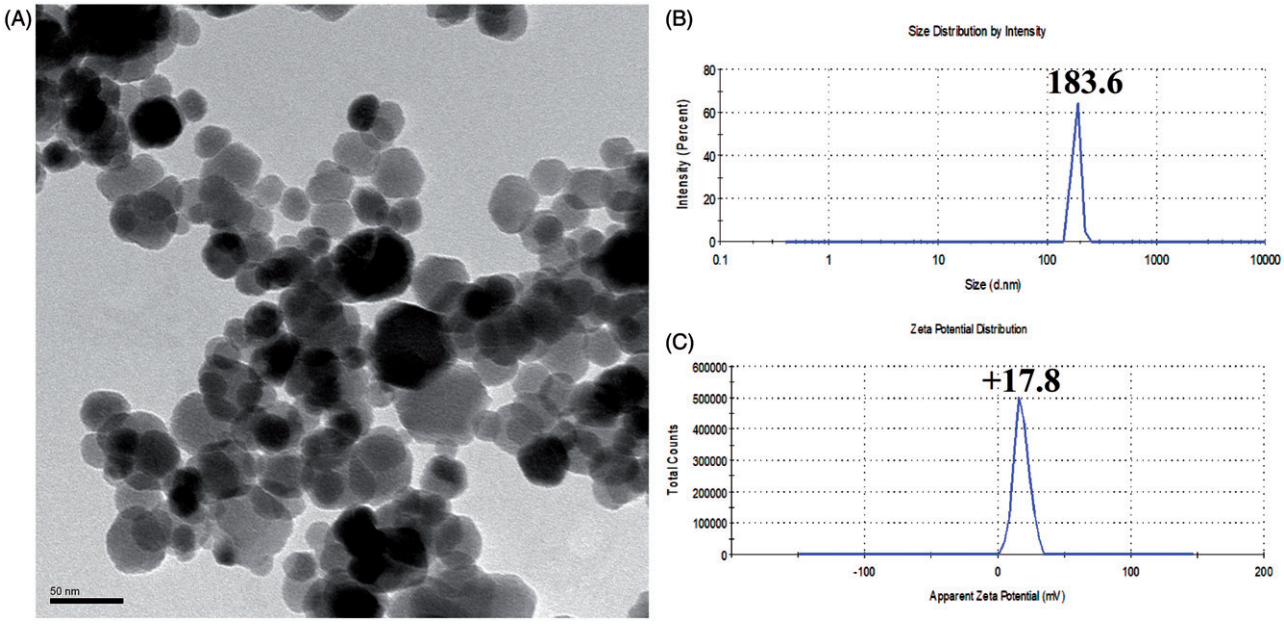

Figure 1. Characterization of Fe_3O_4 NMs by (A) TEM, (B) size distribution and (C) Zeta potential.

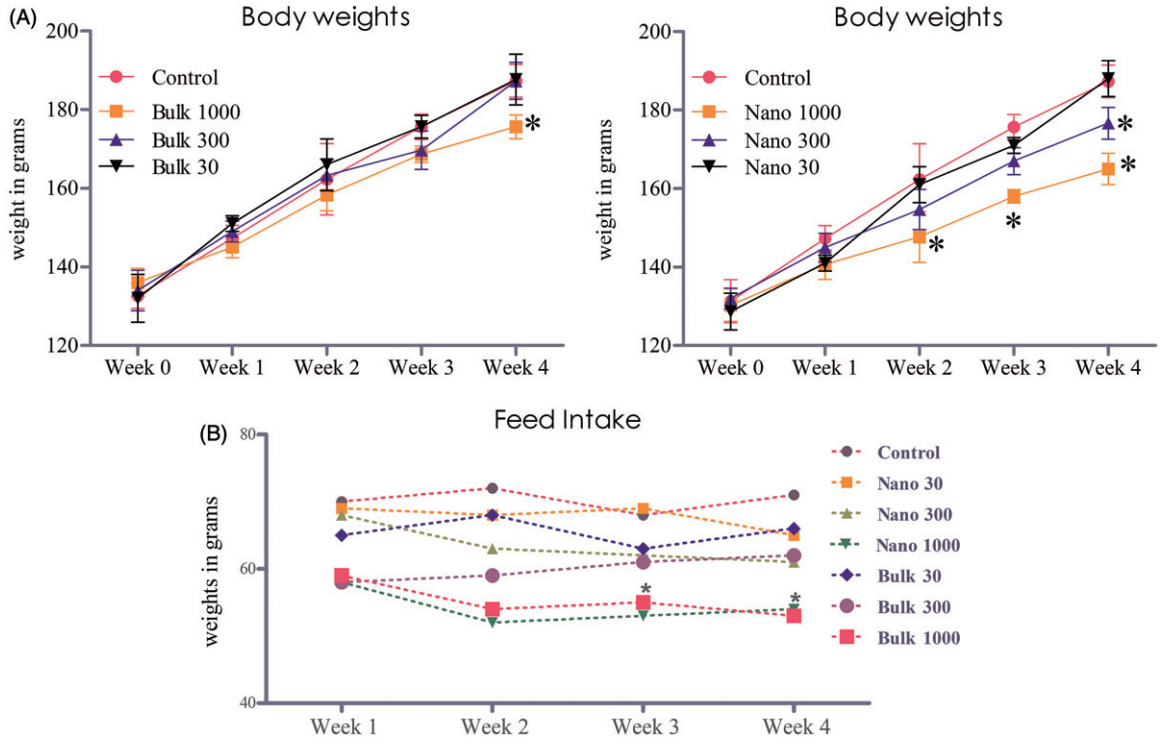

Figure 2. (A) Effect of Fe_3O_4 NMs and its bulk on body weights of animals. (B) Effect of Fe_3O_4 NMs and its bulk on feed intake of animals. Each value represents the mean ± SD; $n = 5$ rats.

of inhibition of pyrogallol auto-oxidation was recorded at 420 nm. Unit enzyme activity was calculated as the amount of enzyme required to give 50% inhibition of pyrogallol auto oxidation.

The catalase activity was assayed using spectrophotometric method of Aebi (1984). In total, 3 ml of 0.063% H_2O_2 in KPB was mixed with 100 µl of tissue supernatant. The change in absorbance was recorded for 1 min at 240 nm. Unit enzyme activity was calculated as micromoles of H_2O_2 decomposed per minute per milligram protein using a molar extinction coefficient of 43.6 M^{-1} cm^{-1}.

The Glutathione peroxidase (GPx) activity was measured using the procedure of Paglia and Valentine (1967). Totally, 750 µl KPB, 60 µl 2.25 mM β-NADPH (β-Nicotinamide adenine dinucleotide phosphate), 15 µl glutathione reductase (GR; 7.1 µl/ ml) and 25 µl GSH (11.52 mg/ ml) were taken in a cuvette. The enzymatic reaction was initiated by adding 100 µl supernatant and 100 µl hydrogen peroxide (1.5 mM). The decrease in absorbance was recorded for 1 min at 340 nm. Unit enzyme activity was calculated as micromoles of β-NADPH oxidized per minute using extinction coefficient of 6.22×10^3 mM^{-1} cm^{-1}.

The GR activity was assayed using the method of Carlberg and Mannervik (1985). A total of 3 ml of reaction mixture contained KPB, 1.0 mM oxidized GSH, 0.15 mM β-NADPH, 0.01% bovine serum albumin and 100 µl tissue supernatant were added. The change in the absorbance was recorded at 340 nm. Molar extinction coefficient of 6.22×10^3 mM^{-1} cm^{-1} was used to calculate GR activity.

The Glutathione-S-transferase (GST) activity was determined according to the method of Habig *et al.* (1974). A total of 2.7 ml KPB, 100 µl 75 mM GSH, 100 µl 30 mM CDNB (1-chloro-2,4-dinitrobenzene) and 100 µl supernatant were taken in a tube. The change in absorbance was recorded at 340 nm for 1 min. The unit enzyme activity was expressed as micromoles CDNB-conjugate per minute per millgram protein using a molar extinction coefficient of 9.6×10^3 M^{-1} cm^{-1}.

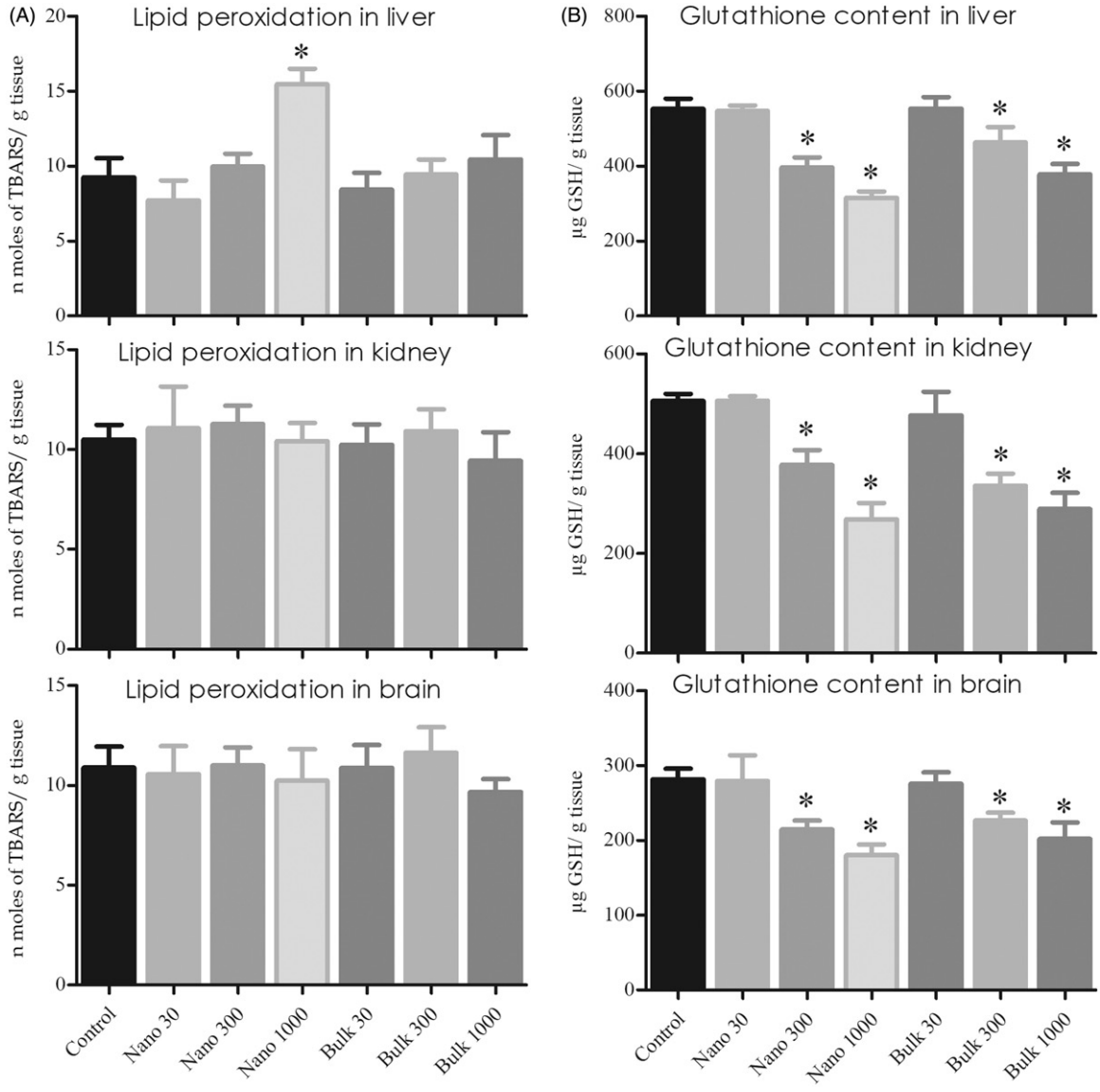

Figure 3. Effect of Fe_3O_4 NMs and its bulk on (A) TBARS and (B) GSH levels in liver, kidney and brain after 28 d of repeated oral treatment. Each value represents the mean ± SD; $n = 5$ rats. $^*p < 0.05$.

Histopathological examination

A small section of liver, kidney and brain were collected from treated and control rats, fixed in 10% buffered formalin overnight. The tissues were dehydrated in ascending concentrations of ethanol and cleared in benzene using Leica TP 1020 tissue processor, followed by embedding in paraffin blocks using Leica EG 1160 paraffin embedder. Using microm HM 360 microtome, paraffin blocks were cut into 5-µm thick sections and fixed on slides. These sections were deparaffinized using xylene, ethanol and stained with hemotoxylin and eosin (H&E) in Microm HMS-70 stainer. The slides were observed under optical microscope (Olympus BX51, Japan).

Tissue distribution

A total of 0.1–0.3 g of liver, kidney, brain and feces and 0.1 ml of urine from the treated and control rats were predigested in nitric acid overnight. Samples were then heated at 80 °C for 10 h followed by heating at 130–150 °C for 30 min. A total of 0.5 ml of 70% perchloric acid was added. The samples were reheated for 4 h, and evaporated nearly to dryness. Subsequently, these solutions and urine (0.5 ml) samples were made up to 5 ml with deionized water and filtered (Reddy *et al.* 2015). Iron standard was diluted to 1, 10, 50, 100 ppm for standardization and validation of ICP-OES (IRIS Intrepid II XDL, Thermo Jarrel Ash) and analyzed the metal content in samples.

Statistical analysis

The results are presented as the mean ± (SD) of number of observations. Comparisons of means were carried out using one-way analysis of variance (ANOVA) followed by Dunnett's multiple comparison test to compare means between the different treatment groups using Graph Pad prism (Graph pad Software, San Diego, CA, USA). Differences were considered significant at $p < 0.05$.

Results

Characterization

Detailed physicochemical characterizations of the Fe_3O_4 NM used in this study are summarized in Figure 1. TEM analysis revealed that Fe_3O_4 NM was monodisperse and spherical in shape having a mean diameter of 29.6 ± 12.2 nm. The mean hydrodynamic diameter of NM dispersed in water as measured by DLS was 183.6 nm which is six folds larger when compared to TEM size suggesting particles were agglomerated. Polydispersity index (PDI) value of 0.582 represents that the NMs were polydisperse. Zeta potential indicates electrical stability of NMs in colloidal dispersions; values less than ≤5 mV specify a lack of sufficient repulsion leading to

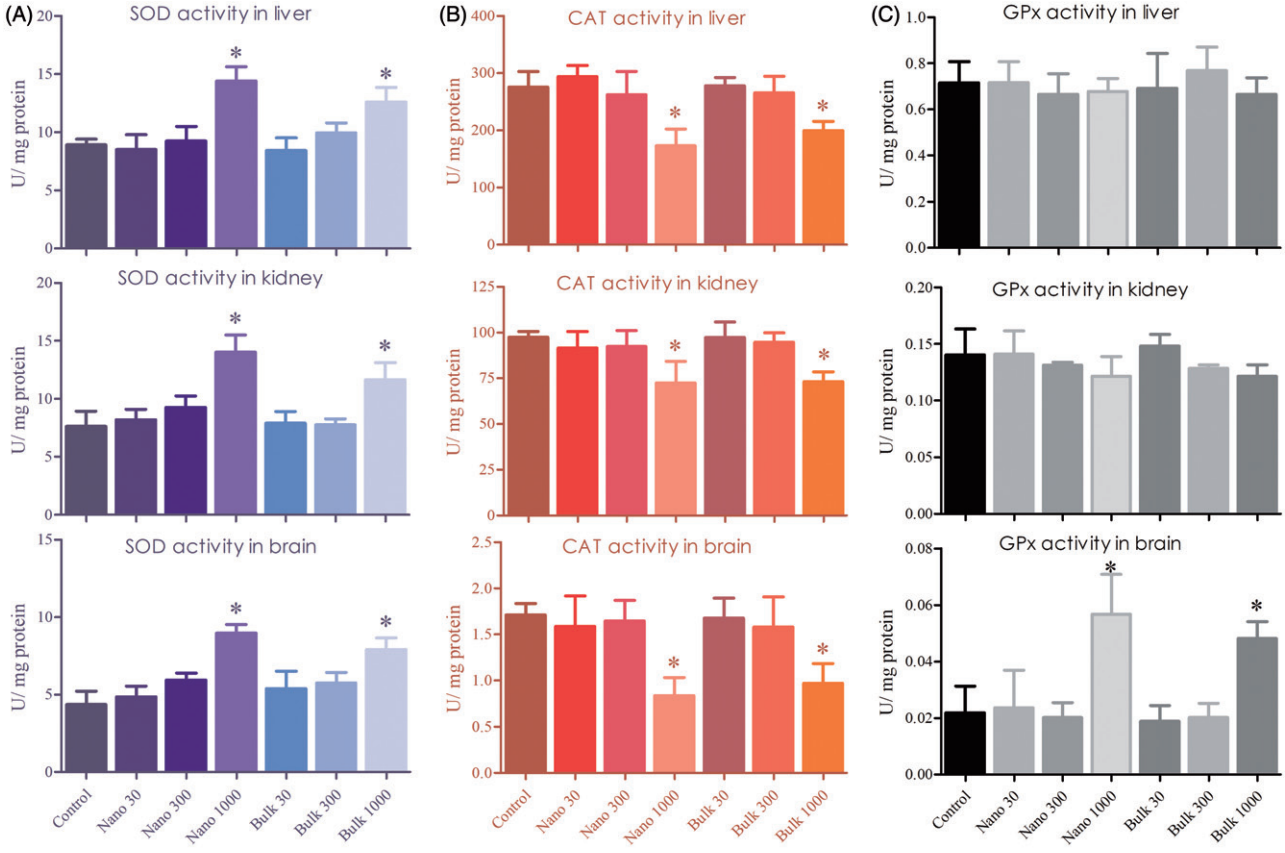

Figure 4. Effect of Fe_3O_4 NMs and its bulk on enzyme activities of (A) Superoxide dismutase, (B) Catalase and (C) Glutathione peroxidase in liver, kidney and brain of rats after 28 d of repeated oral treatment. Each value represents the mean ± SD; $n = 5$ rats. $^*p < 0.05$.

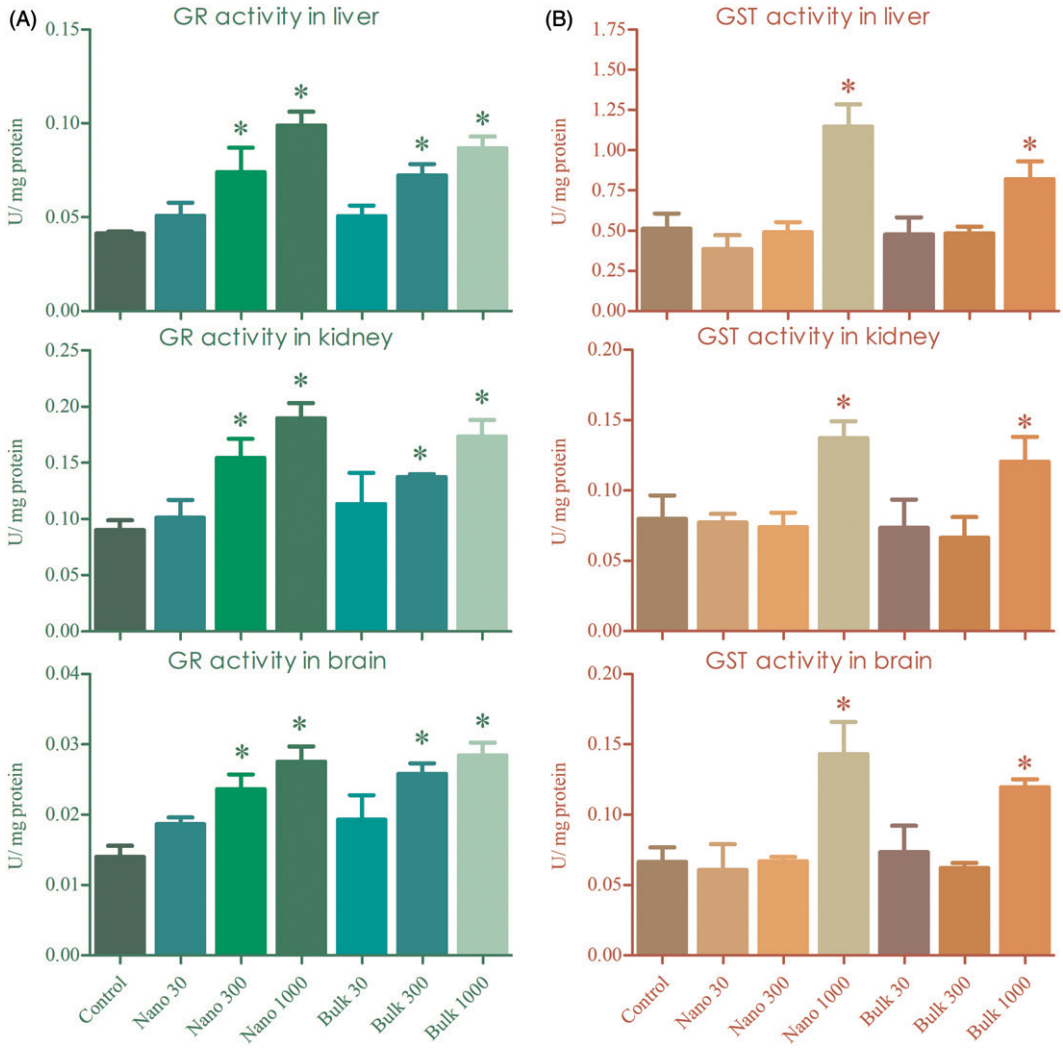

Figure 5. Effect of Fe_3O_4 NMs and its bulk on enzyme activities of (A) Glutathione reductase and (B) Glutathione-S-transferase in liver, kidney and brain of rats. Each value represents the mean ± SD; $n = 5$ rats. $^*p < 0.05$.

coagulation. The ζ potential of NMs was +17.8 mV at pH 7, which corresponds to the pH of natural water.

Body weights and feed intake

The effect of Fe_3O_4 NMs and bulk treatment for 28 d on body weights of the rats is presented in Figure 2(A). The results revealed that the Fe_3O_4 NMs treatment at high dose significantly decreased the body weight of the rats from week 2, week 3 and week 4. Further, Fe_3O_4 NMs medium dose group rats showed significant decrease in body weight in week 4. However, Fe_3O_4 bulk treatment brought significant decrease in body weight only in week 4 of high dose group rats. It was observed that the effect of Fe_3O_4 NMs was more significant in reducing body weight gain than the bulk. Moreover, the feed intake was significantly reduced in high-dose treated animals of bulk and nano group in week 2, 3 and 4, respectively.

Oxidative stress biomarkers

Fe_3O_4 NMs treatment showed significant increase in the amount of TBARS only in liver at 1000 mg/kg dose level. However, bulk at high dose did not show any significant difference in TBARS levels of treated and control groups. Both Fe_3O_4 NMs and bulk at medium and low dose group rat tissues showed no change in the TBARS levels when compared to control. It was observed that the induction of LPO was more significant in NM-treated group than its bulk (Figure 3(A)).

In the present study, GSH levels of treated and control rats were measured and shown in Figure 3(B). Both Fe_3O_4 NMs and its bulk treatment at high and medium dose levels resulted in dose-dependent depletion of GSH levels in liver, kidney and brain. However, Fe_3O_4 NMs and bulk treatment at low dose did not alter GSH levels in the tissues. It was also witnessed that NM treatment brought more severe effect on GSH depletion than the bulk.

Figure 4(A) represents the activity of the superoxide dismutase (SOD) in various tissues of the experimental animals. Our study reveals that nano and bulk Fe_3O_4 administration repeatedly for 28 d brought significant increase in SOD activity in liver, kidney and brain at 1000 mg/kg dose. Low and medium groups of both nano and bulk Fe_3O_4 did not show any change in SOD activity.

The CAT activity was assayed in control and treated rats and the results are presented in Figure 4(B). Fe_3O_4 NMs and

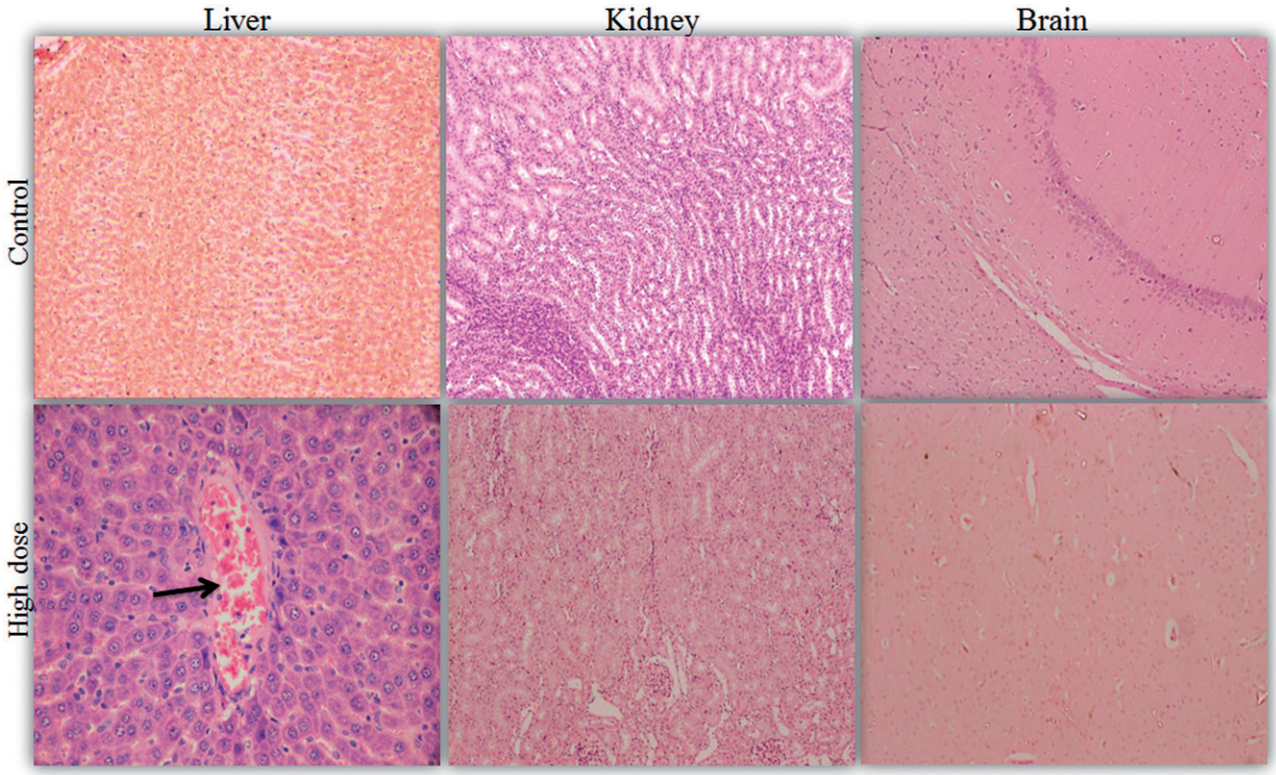

Figure 6. Normal architecture of liver, kidney and brain from control rats were shown in upper panel. Lower panel represents liver, kidney and brain from high dose group treated with Fe_3O_4 NMs showing pathological changes pointed by arrows. Observations were made at 40× magnification.

its bulk treatment at 1000 mg/kg dose resulted in significant decrease in the CAT activity in the liver, kidney and brain. However, 30 and 300 mg/kg dose levels did not cause any change in CAT activity. However, significant effect in inhibiting CAT activity was higher in Fe_3O_4 NMs-treated rats than the bulk.

Effect of Fe_3O_4 NMs and bulk on GPx activity after oral treatment for 28 d in various tissues is presented in Figure 4(C). Fe_3O_4 NMs and bulk treatment did not result in any significant change in GPx activity in liver, kidney and brain of rats from all the dose levels.

The GR activity was assayed in control and Fe_3O_4 NMs and bulk treated rats and are presented in Figure 5(A). Repeated oral treatment of rats with Fe_3O_4 NMs and bulk for 28 d had significantly increased the GR activity at medium and high dose groups in a dose-dependent manner. However, low dose group rats did not show any change in the GR activity.

The GST activity was assayed in various tissues of control and treated rats and are presented in Figure 5(B). The study revealed that both Fe_3O_4 NMs and bulk treatment at 1000 mg/kg significantly induced GST activity in liver, kidney and brain. However medium and low dose group rats showed no significant change in GST activity in all the tissues.

Histopathology

Histopathological changes in liver, kidney and brain tissues of Fe_3O_4 NMs and bulk treated rats after 28 d repeated oral treatment is presented in Figure 6. Only liver from Fe_3O_4 NMs at 1000 mg/kg dose group rats showed histopathological changes such as central venous congestion. However, medium and low dose group rats of Fe_3O_4 NMs and bulk did not show any changes in the histomorphology.

Tissue distribution

The tissue distribution of Fe_3O_4 NMs and bulk in various tissues of rats and their elimination through urine and feces after 28 d repeated oral treatment is presented in Figure 7. The study revealed that both the compounds passed through gastro intestinal tract, reached blood stream and distributed well in liver, kidney and brain of treated rats in a dose-dependent manner. The tissue distribution of Fe was more in high dose rat tissues followed by medium and low dose groups. The accumulation pattern was size dependent, i.e. nano-sized Fe_3O_4 accumulated more significantly than its bulk in all the tissues. The accumulation of both the compounds was found to be more in liver followed by kidney and brain. It was also observed that because of the large size Fe_3O_4 bulk eliminated more through feces than the nano-sized Fe_3O_4. Fe_3O_4 NMs after absorbing through the gut was mostly eliminated through urine than its bulk.

Discussion

In the present study, TEM analysis revealed average diameter of Fe_3O_4 NMs was 29.6 ± 12.2 nm when dispersed in water, NMs agglomerated resulting in increase in size by six folds, i.e. 183.6 nm. The agglomeration of nanoparticles was due to van der Waal's force between individual particles and also the low ionic charge on particles surface was insufficient to stabilize the particles via repulsive force, resulting in

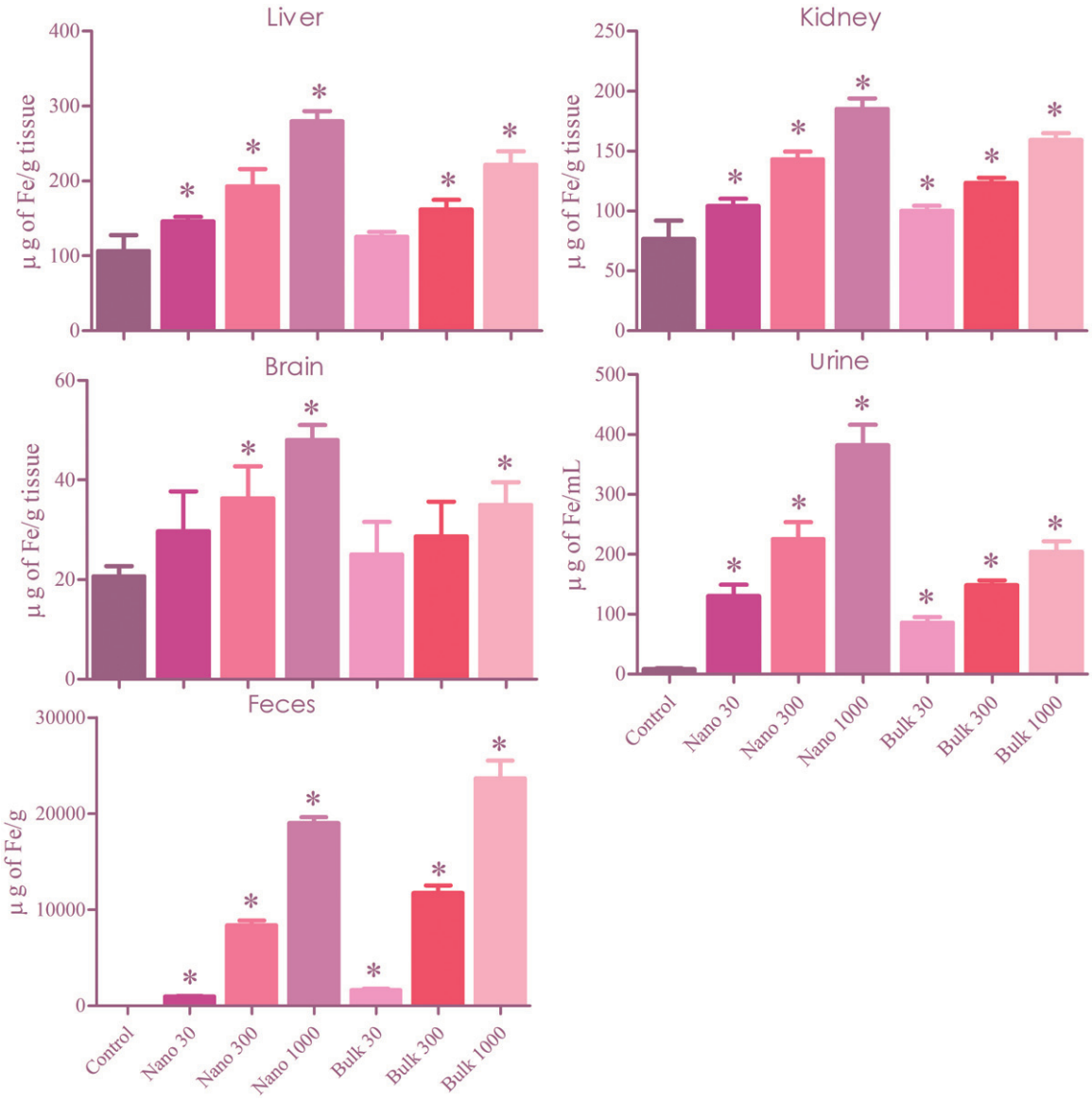

Figure 7. Metal content analysis in liver, kidney, brain, urine and feces of rats after 28 d of repeated oral treatment with Fe_3O_4 NMs and its bulk. * $p < 0.05$.

agglomeration. The aggregates were not much influenced by Brownian movement, resulting in precipitation. Hence, the suspension was sonicated for making stable solution before treatment.

In this study, both Fe_3O_4 NMs and bulk at high dose induced significant lipid peroxidation which suggests that both the compounds fortified ROS generation leading to membrane damage in treated rat tissues. On the other hand, Fe_3O_4 NMs and bulk treatment caused significant dose-dependent decrease of GSH content in treated rat organs. Moreover, rabbits treated with Fe_3O_4 NMs for 14 d resulted in significant depletion in GSH levels with a concomitant increase in LPO in brain cortex (Chahinez *et al.* 2016). This might be due to the reason that GSH directly reacts and nullifies ROS, which also gets utilized in various antioxidant/detoxification processes. Enhanced LPO and decreased GSH in the cell represent oxidative stress condition. It was observed that Fe_3O_4 NMs and bulk treatment brought increase in SOD activity and decrease in CAT activity significantly. Increased SOD activity can be attributed to the cell's response towards increased superoxide radical (O_2^-). However, it may be understood that the increase in the activity of SOD is not sufficient to detoxify the excess of superoxide anion. This is evidenced by the decrease in CAT activity because increased O_2^- may directly inhibit CAT activity (Reddy *et al.* 2015). A higher activity of GR was observed in Fe_3O_4 NMs and bulk treated rat organs in response to excess ROS for the restoration of cellular GSH content. Fe_3O_4 NMs and bulk treatment significantly increased GPx activity in all the tissues, which could be due to defensive response towards increased lipid peroxides. Moreover, the observed increase in GPx activity in the present work correlates well with the significant enhancement in LPO as well as the GSH depletion. On the other hand, GST metabolizes a variety of xenobiotics by conjugating them to GSH. In Fe_3O_4 NMs and bulk treated rats, GST activity was elevated in liver, kidney and brain. This increased activity of GST is also another reason for depleted GSH content as GST utilizes GSH in

conjugation process. On the whole, the oxidative stress biomarkers revealed that the nano-sized Fe_3O_4 induced more significant oxidative stress when compared with its bulk at high dose.

Biodistribution study revealed that along with the increase in doses the accumulation of both Fe_3O_4 NMs and bulk in treated rat organs was increased. Deposition of both the compounds was found high in liver followed by kidney and brain. It was also observed that even though both the compounds were administered at same concentration, there was difference in tissue distribution. In addition, iron overload was well tolerated by both the groups. However, similar results were obtained by Reddy *et al.* (2017) after 28-day repeated oral exposure of IONPs. Stabilized NMs were accumulated more in liver of zebra fish in comparison to bare Fe_3O_4 NMs suggesting stabilized NMs are easily transportable than naked NMs. Moreover, the tissue burden of Fe_3O_4 NMs in zebra fish after 7 d exposure did not induce any mortality, as the stress mechanisms were actively involved in nullifying the effect of NMs (Zheng *et al.* 2017). Histomorphological changes were only observed in high-dose NMs treated group causing central vein congestion in liver. The absorptivity of the particles was dependent upon the size, i.e. Fe_3O_4 NMs deposition was higher when compared with the bulk in all the tissues. The same was reflected in excretion study where the large sized bulk was excreted more in feces without getting absorbed through gastro intestinal tract membrane when compared to the NM.

Similar results were observed in previous research articles as well with different biological models and routes of exposure. Rats following continuous 4 h inhalation exposure to Fe_3O_4 NMs at a dose of 640 mg/m^3 showed significant increase in lipid peroxidation, significant decrease in SOD, CAT, GPx activities and GSH content along with histopathological changes in lung tissue (Srinivas *et al.* 2012). Fourteen days of treatment of Fe_3O_4 NMs in rabbits brought significant reduction in enzyme kinetics of SOD, CAT, GPx and GST (Chahinez *et al.* 2016). On contrary, Singh *et al.* (2012) reported that human lymphoblastoid cells treated with uncoated Fe_3O_4 NMs did not induce any oxidative DNA damage and genotoxicity. However, similar difference between nano and bulk in exerting oxidative stress was reported by Prabhakar *et al.* (2012), where acute oral treatment of Al_2O_3 NMs brought more significant oxidative stress and histopathological changes than its bulk. Biodistribution and histopathological changes were observed in treated rat organs after sub-acute oral treatment of IONPs and bulk materials (Reddy *et al.* 2017).

Conclusion

In conclusion, the results indicated that the difference in physicochemical properties between Fe_3O_4 NM and bulk are significantly reflected in their potential in inducing oxidative stress, bioaccumulation and histological changes in treated rat organs. However, to understand the complete underlying mechanism, further studies are required. The present results suggest that we should be cautious towards the potential risk of intentional or unintentional large-scale exposure to Fe_3O_4 NMs.

Disclosure statement

No potential conflict of interest was reported by the authors.

Funding

This work was financially supported by Department of Biotechnology, New Delhi, India [Project no. BT/PR9998/NNT/28/84/2007]. The authors Utkarsh A. Reddy and P. V. Prabhakar thank the Indian Council of Medical Research, New Delhi, for awarding Senior Research Fellowship.

References

Aebi, H., 1984. Catalase. *In:* L. Packer, ed. *Methods in enzymology*. Orlando, FL: Academic Press, 105, 121–126.

Bekaroğlu, M.G., İşçi, Y., and İşçi, S., 2017. Colloidal properties and in vitro evaluation of hydroxy ethyl cellulose coated iron oxide particles for targeted drug delivery. *Materials science and engineering C: Materials for Biological Applications*, 78, 847–853.

Carlberg, I. and Mannervik, B., 1985. Glutathione reductase. *Methods in enzymology*, 113, 484–490.

Cha, R., *et al.*, 2017. Fe3O4nanoparticles modified by CD-containing star polymer for MRI and drug delivery. *Colloids and surfaces. B, biointerfaces*, 158, 213–221.

Chahinez, T., *et al.*, 2016. Toxicity of Fe_3O_4 nanoparticles on oxidative stress status, stromal enzymes and mitochondrial respiration and swelling of *Oryctolagus cuniculus* brain cortex. *Toxicology and environmental health sciences*, 8, 349.

Foth, H., *et al.*, 2012. Safety of nanomaterials. *Archives of toxicology*, 86, 983–984.

Gogoi, M., *et al.*, 2017. Biocompatibility and therapeutic evaluation of magnetic liposomes designed for self-controlled cancer hyperthermia and chemotherapy. *Integrative biology*, 9 (6), 555–565.

Haase, A., *et al.*, 2012. Effects of silver nanoparticles on primary mixed neural cell cultures: uptake, oxidative stress and acute calcium responses. *Toxicological sciences*, 126, 457–468.

Habig, W.H., Pabst, M.J., and Jakoby, W.B., 1974. Glutathione S-transferases. The first enzymatic step in mercapturic acid formation. *The journal of biological chemistry*, 249, 7130–7139.

Hjorth, R., *et al.*, 2017. Ecotoxicity testing and environmental risk assessment of iron nanomaterials for sub-surface remediation - recommendations from the FP7 project NanoRem. *Chemosphere*, 182, 525–531.

Jollow, D.J., *et al.*, 1974. Bromobenzene-induced liver necrosis. Protective role of glutathione and evidence for 3, 4-bromobenzeneoxide as the hepatotoxic metabolite. *Pharmacology*, 11, 151–169.

Kurbanoglu, S., Ozkan, S.A., and Merkoçi, A., 2017. Nanomaterials-based enzyme electrochemical biosensors operating through inhibition for biosensing applications. *Biosensors and bioelectronics*, 89, 886–898.

Li, K., Nejadnik, H., and Daldrup-Link, H.E., 2017. Next-generation superparamagnetic iron oxide nanoparticles for cancer theranostics. *Drug discovery today*, 22 (9), 1421–1429.

Liu, J., *et al.*, 2017. Fe_3O_4-based PLGA nanoparticles as MR contrast agents for the detection of thrombosis. *International journal of nanomedicine*, 12, 1113–1126.

Lowry, O.H., *et al.*, 1951. Protein measurement with the Folin-phenol reagent. *Journal of biological chemistry*, 193, 265–275.

Lu, J., *et al.*, 2017. Nano iron oxide impregnated in chitosan bead as a highly efficient sorbent for Cr(VI) removal from water. *Carbohydrate polymers*, 173, 28–36.

Ma, B., *et al.*, 2017. Magnetic Fe_3O_4 nanoparticles induced effects on performance and microbial community of activated sludge from a sequencing batch reactor under long-term exposure. *Bioresource technology*, 225, 377–385.

Ma, P., *et al*., 2012. Intraperitoneal injection of magnetic Fe_3O_4-nanoparticle induces hepatic and renal tissue injury via oxidative stress in mice. *International journal of nanomedicine*, 7, 4809–4818.

Marklund, S. and Marklund, G., 1974. Involvement of the superoxide anion radical in the autoxidation of pyrogallol and a convenient assay for superoxide dismutase. *European journal of biochemistry*, 47, 469–474.

Nanotechproject.org, 2015. Available from: www.nanotechproject.org/cpi/ [Accessed March 2015].

Naqvi, S., *et al*., 2010. Concentration-dependent toxicity of iron oxide nanoparticles mediated by increased oxidative stress. *International journal of nanomedicine*, 5, 983–989.

Nigam, S., *et al*., 2017. Near-infrared induced phase-shifted ICG/Fe_3O_4 loaded PLGA nanoparticles for photothermal tumor ablation. *Scientific reports*, 7 (1), 5490.

Novotna, B., *et al*., 2012. Oxidative damage to biological macromolecules in human bone marrow mesenchymal stromal cells labeled with various types of iron oxide nanoparticles. *Toxicology letters*, 210, 53–63.

OECD guideline 407, 2008. *Guideline for the testing of chemicals: repeated dose 28-day oral toxicity study in rodents*. Paris, France: Organization for Economic Cooperation and Development.

Paglia, D.E. and Valentine, W.N., 1967. Studies on qualitative and quantitative characterization of erythrocytes glutathione peroxidase. *The journal of laboratory and clinical medicine*, 70, 158–169.

Prabhakar, P.V., *et al*., 2012. Oxidative stress induced by aluminum oxide nanomaterials after acute oral treatment in Wistar rats. *Journal of applied toxicology*, 32, 436–445.

Ramesh, V., *et al*., 2012. Magnetite induces oxidative stress and apoptosis in lung epithelial cells. *Molecular and cellular biochemistry*, 363, 225–234.

Reddy, U.A., *et al*., 2015. Biomarkers of oxidative stress in rat for assessing toxicological effects of heavy metal pollution in river water. *Environmental science and pollution research*, 22 (17), 13453–13463.

Reddy, U.A., Prabhakar, P.V., and Mahboob, M., 2017. Biomarkers of oxidative stress for in vivo assessment of toxicological effects of iron oxide nanoparticles. *Saudi journal of biological sciences*, 24 (6), 1172–1180.

Shen, J.M., *et al*., 2017. Heterogeneous dimer peptide-conjugated polylysine dendrimer-Fe3O4 composite as a novel nanoscale molecular probe for early diagnosis and therapy in hepatocellular carcinoma. *International journal of nanomedicine*, 12, 1183–1200.

Siddiqui, S.I. and Chaudhry, S.A., 2017. Iron oxide and its modified forms as an adsorbent for arsenic removal: a comprehensive recent advancement. *Process safety and environmental Protection*, 111, 592–626.

Singh, N., *et al*., 2012. The role of iron redox state in the genotoxicity of ultrafine superparamagnetic iron oxide nanoparticles. *Biomaterials*, 33, 163–170.

Srinivas, A., *et al*., 2012. Oxidative stress and inflammatory responses of rat following acute inhalation exposure to iron oxide nanoparticles. *Human & experimental toxicology*, 31, 1113–1131.

Wills, E.D., 1969. Lipid peroxide formation in microsomes. Relation of hydroxylation to lipid peroxide formation. *Biochemical journal*, 113, 333–341.

Zhang, X., *et al*., 2016. Iron oxide nanoparticles induce autophagosome accumulation through multiple mechanisms: lysosome impairment, mitochondrial damage, and ER stress. *Molecular pharmaceutics*, 13 (7), 2578–2587.

Zhao, S., *et al*., 2014. Superparamagnetic iron oxide magnetic nanomaterial-labeled bone marrow mesenchymal stem cells for rat liver repair after hepatectomy. *The journal of surgical research*, 191 (2), 290–301.

Zheng, M., Lu, J., and Zhao, D., 2017. Effects of starch-coating of magnetite nanoparticles on cellular uptake, toxicity and gene expression profiles in adult zebrafish. *Science of the total environment*, 8, 622–623:930–941.

Zhu, M.T., *et al*., 2008. Comparative study of pulmonary responses to nano- and submicron-sized ferric oxide in rats. *Toxicology*, 247, 102–111.

Zhu, S., *et al*., 2017. Developmental toxicity of Fe_3O_4 nanoparticles on cysts and three larval stages of *Artemia salina*. *Environmental pollution*, 230, 683–691.